The Effect of Oil Extraction on Porosity and Methane Adsorption for Dry and Moisture-Equilibrated Shales

Wei Li[1], Lee A. Stevens*[1], Will Meredith[1], Clement N. Uguna[1], Christopher H. Vane[2], Bo Zhang[3], Andrew D. Carr[4], Dingye Zheng[5], Colin E. Snape[1]

1. University of Nottingham, Low Carbon Energy and Resources Technologies Group, Faculty of Engineering, Energy Technologies Building, Triumph Road, Nottingham NG7 2TU, UK.
2. British Geological Survey, Centre for Environmental Geochemistry, Keyworth, Nottingham NG12 5GG, UK.
3. Schlumberger Technologies (Beijing) Ltd, Beijing 100000, China.
4. Advanced Geochemical Systems Ltd., 1 Towles Fields, Burton-on-the-Wolds, Leicestershire LE12 5TD, UK.
5. State Key Laboratory of Petroleum Resources and Prospecting, China University of Petroleum (Beijing), Beijing, 102249, China.

* Corresponding author, Lee.Stevens@nottingham.ac.uk

Abstract

The porosity and methane adsorption capacity of shale used to estimate gas in place (GIP) are affected both by moisture and oil residing in the pore structure, as well as oil naturally present from maturation, which can include contaminant drilling mud fluids used for drilling. To demonstrate the impact of extractable oil on methane adsorption capacity for both dry and moisture-equilibrated shales, two overmature shales from China (SH1, SH2) and two lower mature shales from UK (BS3, GH4) have been investigated. The oils extracted from the overmature shales (<0.5 wt.% TOC) are in low yield and arise from oil-based drilling mud, while the much higher yields from the lower maturity UK shales (1.1-2.5 wt.% TOC) is mainly from oil generated by maturation. After extraction, minimal

changes (<5%) in total nanopore volume (<100 nm) were observed for the dry over mature shales, but significant increases (95 and 176%) were observed for the dry lower maturity shales. More than 60% of the extracted oil resides in micro and mesopores, and removal could unblock the micropore necks and enlarge the accessible meso and macropore volume. Moisture contents are lower for extracted shales, with reductions of 7-37% observed. Methane equilibrium adsorption capacities increased after oil extraction for both the dry and wet shales, especially for lower maturity shales, where increases were over 200% for the wet shales. Henry's Law was used to show that there were not significant amounts of dissolved methane in oils for the dry shales. Extracting oil from shales prior to determining the porosity and methane adsorption capacity can lead to the GIP being over-estimated for moisture equilibrated shales, particularly for oil-window shales where an overestimation of 22% was obtained for the shale investigated in this study. These findings provide a better understanding of the combined impacts of residual oil and water on GIP and avoid its overestimation.

Key words: Shale; Maturity; Oil extraction; Methane adsorption; Gas in place.

Highlights:

1. Over 60% extractable oil from oil-window shale is stored in the micro-mesopores.
2. Oil extraction has limited impacts on overmature dry shales.
3. Moisture contents of wet shales reduce by 7-37% after oil extraction.
4. Extraction increases micropore and methane adsorption capacities up to 282%.
5. GIP for oil-window shale can be over-estimated up to 22% by extracting the oil.

1. Introduction

Accurate shale gas reserve evaluations are valuable for gas exploration [1-5]. Free gas is stored in the available pore volume, adsorbed gas is mainly in micropores with the greatest surface area, and some gas can dissolve in any hydrocarbon and or water [2-4, 6, 7]. Pore networks in shale control the storage and migration of hydrocarbons [1, 8]. The accurate determination of adsorbed gas capacity and porosity is essential for estimating the shale gas in place (GIP) [1-5], both of which can be affected by the residual oil in target shales [9-12]. The impact of extracted oil has not been studied on shales at moisture-equilibrated (wet) conditions, although moisture is not a negligible factor for GIP estimation [5, 8]. Understanding the effect of extractable oil on porosity and gas adsorption, comparing the GIP in all conditions ((initial, extracted, dry and wet) shale can provide guidance for establishing more accurate shale gas reserve estimations.

The organic matter in shales comprises mainly the insoluble organic matter, kerogen (typically > 90%), with small amounts of extractable bitumen or oil (typically <10%) [13] removed with common organic solvents [9, 11, 14]. Thermal maturity is the critical parameter to indicate the evolution stages of shale oil and gas generation [15, 16]. Shale can be categorized as thermally immature, oil mature, gas or high mature, and post or over-mature in terms of capability to generate hydrocarbons [15-17]. Immature shales with vitrinite reflectance (VR) less than 0.5% Ro, may generate biogenic natural gas. Shales with VRs ranging from 0.5 to 1.3% Ro are in the 'oil window'. High maturity shales, with VR in the range 1.3-2% Ro are in the 'gas window' and will generate mainly relatively wet gas, while overmature shales (VR>2% Ro) will generate only dry gas [15-17].

Both initial [6, 18-20] and solvent extracted [8, 21] shales have been used to relate key factors, including temperature, pressure, composition, and moisture impact on the methane adsorption capacity. The difference between initial and extracted dry shales on porosity and methane adsorption capacity has been studied recently [9, 10, 12, 22-24]. Solvent extraction increases

specific surface area (SA) [23, 25]. Methane adsorption in shales can potentially be affected by methane dissolving in any oil present [10, 12, 22-24]. Apart from natural oil arising from maturation [11, 12], oil-based drilling muds, in particular, can also impact methane adsorption and gas dissolution [26]. Oil-based drilling muds are widely used as they do not hydrate active clay minerals, and they can affect further analysis unless proper cleaning methods are applied [14, 27]. Previous researchers have reported that the methane adsorption capacities of the dry extracted shales are larger than for the initial shales [12, 22, 23, 25]. As an example, shales were wiped with dry cloths to remove any drilling fluids before extraction [28]. Different extractive solvents (acetone, tetrahydrofuran (THF), carbon disulfide (CS_2), and benzene) have different impacts on extraction yields since they have different molecular dynamic diameter, aromaticity, boiling point, and polarity, which can lead to various effects on porosity and methane adsorption. However, all these studies on the impact of solvent extraction on methane adsorption and pore characteristics of shales were carried out on dry shales [12, 22, 23, 25] .

Water exists under reservoir conditions and moisture significantly reduces the methane adsorption for coals and shales [29-32], making researchers focus on moisture equilibrated shales [3, 8, 33-37]. Water reduces gas adsorption by occupying pore volume and blocking the pore necks, and the GIP estimated for moisture-equilibrated shale is considered more accurate [5, 8]. Gas adsorption for wet shales before and after solvent extraction could be different due to the combined influence of moisture and oil on the pore network. However, to date, the combined impact of moisture and residual oil on the porosity and methane adsorption capacities of shales has not been investigated. Furthermore, for dry shales, previous studies have not addressed the influence of extractable oil on GIP estimates [9, 10, 12].

In this study, high-pressure methane adsorption and low-pressure gas sorption were carried out for dry and moisture-equilibrated shale before and after solvent extraction. For the first time, the

impacts of solvent extraction on GIP estimations for both dry and moisture-equilibrated shales are revealed. For the shales investigated, the difference between extractable oil that arises from maturation, and that introduced as contaminants from oil-based drilling mud is emphasized.

2. Experimental Methods

2.1 Sample Preparation

Two over-mature shales from China were collected from Ordovician-Lower Silurian Wufeng-Longmaxi Formation, south of Sichuan Basin, with the depth of 4119 m for shale 1 (SH1) and 4098 m for shale 2 (SH2). SH1 and SH2 were selected from different drilling wells [5]. Two lower mature shales from the UK were collected from the Carboniferous Bowland basin, Becconsall (BS3) from a depth of 2143 m, and Grange Hill (GH4) from a depth of 3113 m. To minimize the effect of sample heterogeneity for the following experiments, all the prepared core shales were crushed and sized to 2-4 mm. For solvent extraction, aliquots of the 2-4 mm particles were further crushed to <250 µm for comparison.

The initial and solvent extracted shale samples were both dried and equilibrated at 95% relative humidity (R.H.) moisture (wet) for high-pressure and low-pressure gas sorption experiments. The dry shales were prepared in the vacuum oven (<0.5 mbar) at 120 °C for 48 hours before starting any experiments. The wet shales were prepared in a vacuum desiccator containing saturated potassium nitrate (KNO_3) solution (8 g KNO_3/10 mL H_2O), which can provide 95±2% R.H. moisture equilibration conditions at 20 °C [38-40]. A logger was used to monitor the R.H. and the temperature to make sure the shales reach the moisture equilibration after being kept in the desiccator for 48 hours [5]. The moisture contents for the wet samples were calculated from the mass differences.

2.2 Soxhlet Extraction

Soxhlet solvent extraction was carried out on 20 g of shale using both the 2-4 mm and <250 µm fractions to ensure the particle size has limited impact on the oil yields in this study, as the oil yield similarity is more than 98%. Samples were loaded into the pre-cleaned thimble and plugged with cotton wool to ensure samples remain in the thimble during extraction. A mixture of 186 mL dichloromethane (DCM) and 14 mL methanol was used. Extraction was carried out for 120 hours at 40 °C. The solvent was removed after extraction using a rotary evaporator at 35 °C under 400 mbar pressure. The remaining solvent (about 2 mL) was then collected into a pre-weighed vial and dried at 25 °C until no weight change. The extracted shales were dried in a fume hood for 24 hours, before drying in a vacuum oven (<0.5 mbar) at 120 °C for 48 hours. The extracted organics yield was calculated by the mass of oil and sample TOC. Duplicate extractions for each shale were carried out to collect the remaining solvent (about 2 mL) without drying, which was prepared for the GC-MS analysis.

2.3 Elemental Analysis and Vitrinite Reflectance

Shales prepared for elemental analysis were ground into powder (<250 µm). 3 g of powdered initial shale was treated with sufficient hydrochloric acid (HCl), 1 mol/L, to remove the carbonate. The treated samples were washed with distilled water for 6 times until pH 7 is reached. After carefully decanting the water from the samples, samples were dried in the vacuum oven (<0.5 mbar) at 120 °C for 48 hrs. Then 120 mg of shale was used to determine the total organic carbon (TOC) contents using a Leco CHN628 elemental analyzer. About 1.5 g (2-4 mm particle size) of shale was used to prepare the polished blocks for the VR (% Ro) measurement. The measurement of recognizable vitrinite was done using a LEICA DM4500P microscope with motorized 4-fold turret for reflectance, and data were collected via the Hilgers Fossil Man system connected to the microscope. For the two Chinese over mature shales, bitumen reflectance (BR) measurements were conducted on the

polished blocks because of the lack of vitrinite in the Wufeng-Longmaxi shales. The VR was calculated from the BR according to the Equation (1) [41].

$$VR = \frac{BR + 0.2443}{1.0495} \quad (1)$$

2.4 Low-pressure gas (N_2, CO_2) sorption

Low-pressure gas sorption experiments were carried out on both initial and extracted dry and wet shales (2-4 mm particles) by a Micromeritics Surface Area and Porosity Analyser (ASAP 2420) to obtain the pore characteristics of initial and extracted shales. In this study, Brunauer-Emmett-Teller (BET) theory was used to obtain the surface area (SA) from N_2 sorption, where the relative pressure (P/P°, P is the absolute equilibrium pressure and P° is the saturation pressure) is in the range of 0.05 and 0.2 [42, 43]. Non-Local Density Functional Theory (NLDFT) equilibrium model assuming slit pores was used to calculate the pore volume from 0.33 to 100 nm [7, 44, 45]. Compared with the Barrett-Joyner-Halenda (BJH) model, the NLDFT model can give a more realistic description of micropore filling while using the BJH model is always leading to an underestimation of pore sizes of micropores and even smaller mesopores [43, 46-48]. 4 g dry and wet particle (2-4 mm) shales was used for the low-pressure N_2 sorption experiments, and 2 g dry shale was prepared for CO_2 adsorption.

The shale samples were degassed under high vacuum (<0.013 mbar) at 120 °C for 15 hours before dry low-pressure (N_2, CO_2) sorption experiments. To ensure the wet samples were not exposed to vacuum at higher temperatures, the wet shale samples were frozen in liquid N_2 first before manually evacuating the sample tube and starting the low-pressure N_2 sorption analysis. The mass deviation of wet samples before and after analysis was ±0.002%. The P/P° of low-pressure N_2 sorption analysis is set from 10^{-7} to 0.995 P/P°, and all the analysis was performed at -196 °C in a liquid N_2 bath. The low-pressure CO_2 sorption analysis was carried out at 0 °C with a P/P° from 6×10^{-5} to 3.5×10^{-2}, with

159 absolute pressure is from 0.002 to 1.2 bar, to characterize the ultra-microporous structure (<0.8 nm)
160 of dry shales [8, 49].

161 CO_2 adsorption was not carried out for wet shales because the experimental temperature is 0 °C
162 which is hard to hold the moisture in the wet sample under low pressure. Besides, the difference
163 between N_2 and CO_2 SA on dry samples is <10%, suggesting that N_2 can penetrate most ultra-
164 micropores of wet samples [5]. The free space test by helium on the instrument was not used for
165 the low-pressure gas sorption isotherms since an automatic warm free space test would expose the
166 equilibrated moisture samples to a vacuum which would remove the moisture. Thus, the skeletal
167 densities of wet and dry shales measured by Helium pycnometry were used to calculate the warm
168 and cold free space manually to obtain the correct gas sorption results. The bulk density of dry shales
169 was obtained from Mercury intrusion porosimetry by Micromeritics Autopore IV Series instrument
170 at 0.035 bar, which was conducted from this pressure to 4137 bar [5, 50].

171 ## 2.5 High-pressure methane adsorption

172 A Micromeritics High-Pressure Volumetric Analyzer (HPVA-100) was used to measure the high-
173 pressure methane adsorption of shale by the static volumetric method. Approximately 10 g shale
174 particles (2-4 mm) wet and dry were weighed and loaded into the 10 mL stainless steel sample cell
175 and sealed before the measurement. Each sample was analyzed in triplicate to assess errors. For
176 the dry measurement, all the samples in the cell were degassed at 120 °C for 48 hours first, and then
177 the methane adsorption isotherms were acquired. A sample pre-evacuation was carried out for 45
178 minutes to reach a vacuum setpoint of 0.013 bar on the high-pressure instrument, and an isotherm
179 was generated from 0 to 105 bar with a 45-minute equilibration time per pressure point. For the
180 wet shales, all the methane adsorption isotherms were obtained from 1.2 to 105 bar at 25 °C,
181 avoiding the wet samples being subjected to a vacuum on the high-pressure instrument. The mass
182 deviation of wet shales before and after analysis was ±0.0018%. Similar free space corrections were

carried out on this instrument as for the low-pressure gas sorption method using skeletal density and manually calculating warm and cold free spaces.

The actual adsorbed amount of gas is represented by the absolute amount, and this is the gas quantity that needs to be considered rather than the surface excess amount obtained by the volumetric sorption measurement. The Gibbs equation (Equation (2)) [1, 51] is used to do the conversion, since the difference between excess and absolute amount adsorbed is non-negligible at pressure exceeding 10 bar [7]. The dual-site Langmuir model, which is suitable for heterogeneous adsorbents [1, 8] is used in this study to predict the methane adsorption at pressures over 105 bar. The equation for the dual-site Langmuir can be written in the following form Equation (3).

$$Q_a = Q_e + (V_a \times \rho_g) \quad (2)$$

$$Q_a(P,T) = Q_{max} \times \left[(1-\alpha)\frac{b_1(T)P}{1+b_1(T)P} + \alpha\frac{b_2(T)P}{1+b_2(T)P}\right] \quad (3)$$

Where, Q_a is the absolute adsorption quantity; Q_e is the excess adsorption quantity; Q_{max} is the max absolute adsorption quantity; V_a is the pore volume for gas to adsorb into; ρ_g is the density of the bulk gas; $b_1(T)$ and $b_2(T)$ are the temperature-dependent equilibrium constants, which are related to the energy of adsorption sites; $b_1(T)$ and $b_2(T)$ are weighted by a coefficient (α); α is the fraction of the second type of site ($0 < \alpha < 1$); P is the pressure; T is the temperature.

2.6 Gas Chromatography-Mass Spectrometry

Extracted oils from the shales were analyzed by gas chromatography-mass spectrometry (GC-MS) using an Agilent GC-MS (7890B GC; 5977A-mass selective detector (MSD)) in splitless mode. Product separation was performed on an HP-5MS column (30 m × 250 µm × 0.25 µm). The GC oven temperature was initially held at 50 °C for 0.5 min, then heated to 300 °C at a rate of 4 °C/min, where it was held for 5 minutes. The MS (EI of 70 eV) was scanned in the mass range of m/z 40–400, with an ion source temperature of 200 °C. Individual compounds were identified using a NIST 14 MS library and published data.

3. Results and Discussion

3.1 Shale characterization and geochemistry

Basic information on the shales, including their formation, burial depth, TOC, maturity, moisture content of wet samples, and the yield of extracted oil are listed in Table 1. The shales from different formations and depths have TOC contents ranging from 2.4 to 5.1 wt.%. Shales SH1 (2.95% Ro) and SH2 (2.58% Ro) are overmature, BS3 (1.01% Ro) is oil-window maturity and GH4 (1.95% Ro) is gas-window maturity. The moisture contents of the initial and extracted shales are in the ranges 1.22-2.72 and 1.13-2.06 wt.%, respectively, indicating the extracted shales adsorb less water with reductions of 15, 7, 37, and 25% for SH1, SH2, BS3, and GH4, respectively. The yield of extractable oil decreases with increasing maturity from 2.5 wt.% TOC for the oil-window shale, BS3 to 1.1 wt.% TOC for the gas-window shale, GH4, and 0.3-0.5 wt.% TOC for the over-mature shales, SH1 and SH2. The extracted oil volumes range from 0.13 to 0.73 µL/g, assuming the extracted oil density is 0.85 g/m^3, which is the same as light crude oil [52, 53]. Wufeng-longmaxi shale is dominated by Type II kerogen [54]. Although the Bowland shale is a mixture of Type II/III and IV kerogens [55, 56], the oil has been generated predominately from the Type II kerogen present. The impact of kerogen type is limited, as all the oil in these four shales come from a similar type.

Table 1. Characteristics of the initial and extracted shales

Sample	Formation	Depth (m)	TOC (wt.%)	Maturity (% Ro)	Moisture (wt.%)	Oil yield (wt.% TOC)	Oil volume (V_{oil}) (µL/g)
Initial SH1	Ordovician - Lower Silurian Wufeng-Longmaxi, China	4119	5.1	2.95	1.50[a]	0.3	0.17
Ext SH1					1.27[b]		
Initial SH2	Ordovician - Lower Silurian Wufeng-Longmaxi, China	4098	2.4	2.58	1.22[a]	0.5	0.13
Ext SH2					1.13[b]		
Initial BS3	Carboniferous Bowland Becconsall, UK	2143	2.5	1.01	1.84[a]	2.5	0.73
Ext BS3					1.17[b]		
Initial GH4	Carboniferous Bowland Grange Hill, UK	3113	3.4	1.95	2.72[a]	1.1	0.44
Ext GH4					2.06[b]		

The TOC, moisture, and oil yield were the average data from triplicate determinations. Moisture[a] is the moisture content for the initial shale, and moisture[b] is that for extracted shale.

3.2 GC-MS characterization of the extracted oils

Figure 1 shows the total ion chromatograms (TIC) and m/z 71 single ion chromatograms (EIC 71) for the oils extracted from the four shales with the *n*-alkane peaks labelled. For the two over-mature shales where the extractable oil yields are low, light condensate would be expected with possibly small quantities of residual oil. The oils are relatively heavy and contain *n*-alkanes in low concentrations. However, the fact that the *n*-alkanes do not extend beyond n-C_{23} would suggest that they could arise from a small quantity of remaining oil. *n*-Hexadecane dominant in the extract from SH1 (Figure 1A) is possibly drilling fluid-derived [57]. A similar phenomenon is evident for the extract from SH2 (Figure 1B), where the drilling fluid is causing slightly elevated concentrations of *n*-hexadecane and *n*-octadecane over the other n-alkanes, although much less pronounced [57]. The majority of the TICs for the extracts from the two over-mature shales comprise complex mixtures extending beyond C_{30}. The common drilling mud 'oil' bases including the diesel, enhanced-mineral oil (EMO), and synthetics (olefins and esters). The oil contaminated by the diesel and EMO shows a relatively higher peak of C_{16} in GC data [57]. The evidence would suggest that EMOs account for most of the complex mixtures extracted from SH1 and SH2.

The oil from the oil-window shale, BS3, is characteristic of a paraffinic oil with *n*-alkanes prominent ranging from C_{16} to C_{33} and the pristane to phytane ratio close to 1 (Figure 1C). The yield of oil extracted from the gas-window Bowland shale sample (GH4) was much lower than that for the oil-window shale (BS3) and is considerably lighter with n-alkanes from C_{12} to C_{23} (Figure 1D). Furthermore, there is evidence of some non-hydrocarbon contamination from siloxane and methyl esters which are likely to rise from column bleed and the septa of the GC or the vial cap.

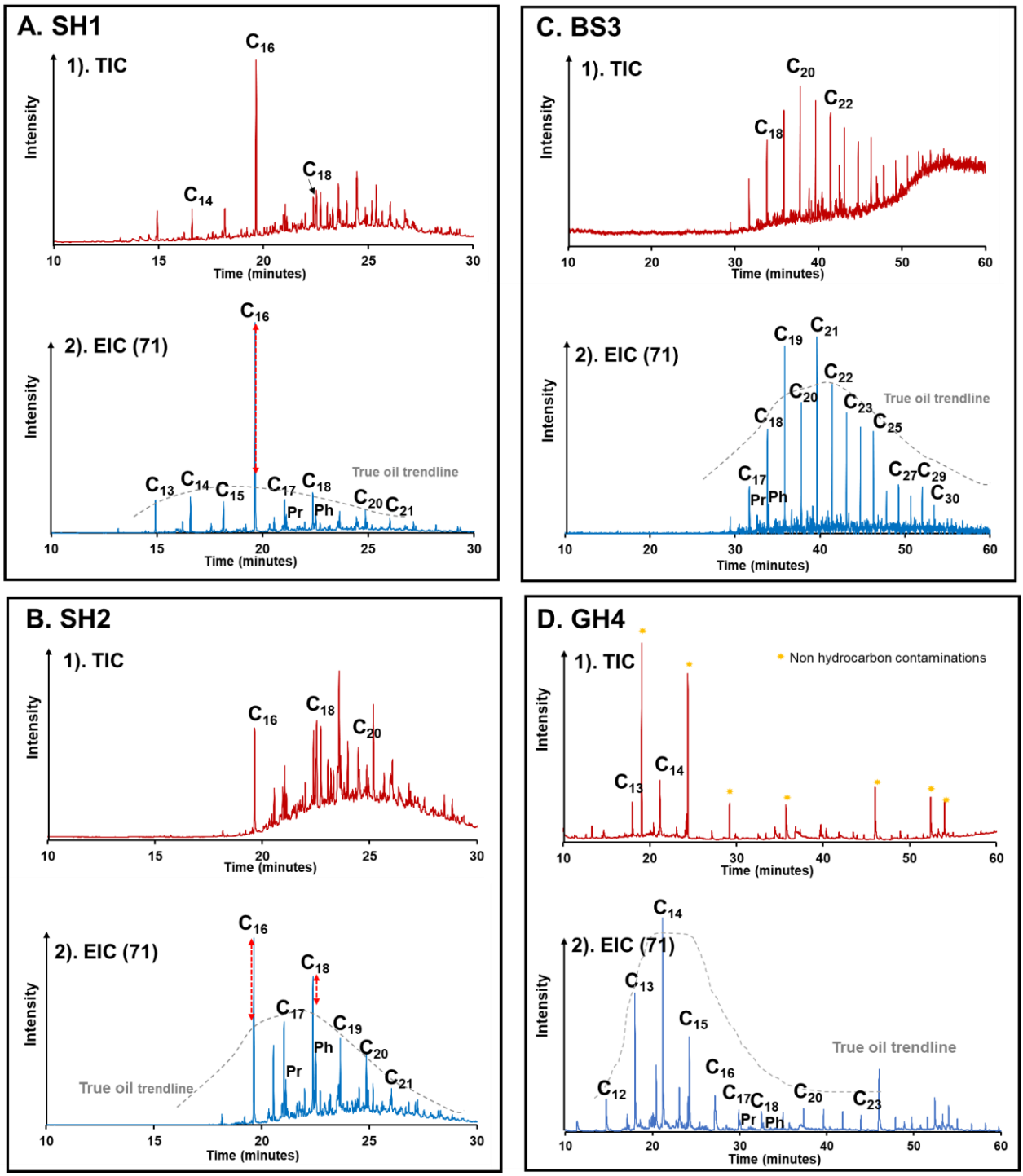

Figure 1. GC-MS total ion and m/z 71 single ion chromatograms for the extracted oil with the *n*-alkane peaks labelled. A, B, C, and D are the oils from SH1, SH2, BS3, and GH4.

3.3 Impact of solvent extraction on nanoporosity

The pore SA, micro (<2 nm), meso (2-50 nm), macro (50-100 nm), total nanopore volumes (<100 nm) [43], and their changes after solvent extraction calculated from the low-pressure N_2 and CO_2 gas isotherms in this research are compared in Table 2. The different pore volume percentages for the

dry and wet initial and extracted shales are presented in Figure 2. The micropore volumes of the dry shales general increase with maturity (Table 2), with the order being oil window (BS3), gas window (GH4), and overmature (SH1>SH2), which is also the case on a TOC basis (SH2>SH1>GH4>BS3). This implies most micropores reside with the organic matter, and high maturity shales developing more pores during hydrocarbon generation [21, 58-61]. Although mesopores are dominant in the dry shales (Figure 2), the micropores still occupy a significant fraction of the pore volume. The contributions of micropores to the total nanopore volume are much higher in the over mature shales, SH1 and SH2, than those in the gas-window shale GH4 and oil-window shale BS3 (Figure 2), suggesting hydrocarbon generation facilitates the development of micropores [61-63].

Increases in pore volume are expected after any native oil is extracted [11, 28]. However, for the dry over mature shales, the changes (<20 %) in surface area and nanopore volume are small (Table 2) due to the low extraction yields (<0.5wt.% TOC, Table 1), with the extracted material being mainly drilling mud derived. Since the permeability of shales (typically less than 0.001 mD) is very low [64] [65] [66], it is difficult for the drilling muds to penetrate the shale bulk, with most being on the surface. Solvent extraction may cause additional effects, such as contributing to the swelling of clay pores by the solvent [67] or changing the interactions with rocks if solvent is adsorbing on clay surfaces or in kerogens [11, 28], which could interrupt the physical interactions between shales and adsorbed gas leading to the measured SA and pore volume decreasing after extraction.

Table 2. Surface area and pore volumes of dry and wet shales.

Sample name	BET SA (m^2/g)	V_{micro} (µL/g TOC)	V_{micro} (µL/g)	V_{meso} (µL/g)	V_{macro} (µL/g)	V_{nano} (µL/g)
Dry Initial SH1	21.73	135	6.9	11.7	0.75	19.3
Dry Ext SH1	19.11	112	5.7	11.8	0.87	18.4
SH1 Change*	**-12%**	**-**	**-17%**	**1%**	**15%**	**-5%**
Dry Initial SH2	16.70	224	5.37	6.7	0.16	12.2
Dry Ext SH2	16.67	226	5.42	6.5	0.14	12.1
SH2 Change*	**-0.2%**	**-**	**1%**	**-2%**	**-17%**	**-1%**
Dry Initial BS3	0.13	3.9	0.098	0.34	0.11	0.55

Dry Ext BS3	0.26	6.4	0.160	0.72	0.20	1.1
BS3 Change*	**92%**	**-**	**64%**	**110%**	**78%**	**95%**
BS3 Oil P*	**-**	**-**	**9%**	**52%**	**12%**	**73%**
Dry Initial GH4	2.19	18	0.60	1.7	0.17	2.4
Dry Ext GH4	2.62	20	0.70	5.3	0.7	6.7
GH4 Change*	**20%**	**-**	**17%**	**222%**	**273%**	**176%**
GH4 Oil p*	**-**	**-**	**23%**	**845%**	**109%**	**977%**
Wet Initial SH1	0.075	0.08	0.0039	0.28	0.063	0.34
Wet Ext SH1	0.059	0.16	0.0081	0.20	0.051	0.26
SH1 Change*	**-21%**	**-**	**105%**	**-28%**	**-19%**	**-25%**
Wet Initial SH2	0.029	0	0	0.21	0.056	0.27
Wet Ext SH2	0.036	0.14	0.0033	0.16	0.042	0.20
SH2 Change*	**25%**	**-**	**-**	**-26%**	**-25%**	**-25%**
Wet Initial BS3	0.060	0	0	0.18	0.038	0.22
Wet Ext BS3	0.108	0	0	0.32	0.07	0.40
BS3 Change*	**79%**	**-**	**-**	**80%**	**98%**	**83%**
Wet Initial GH4	0.011	0	0	0.07	0.023	0.09
Wet Ext GH4	0.045	0.04	0.0012	0.25	0.089	0.34
GH4 Change*	**310%**	**-**	**-**	**257%**	**295%**	**268%**

BET SA are the surface areas calculated by BET theory; V_{micro}, V_{meso}, V_{macro}, and V_{nano} are the micropores (<2 nm), mesopore (2-50 nm), macropore (50-100 nm), and the total nanopore volume (<100 nm) calculated by the NLDFT model. Change* (in bold) is the change in pore properties resulting from solvent extraction compared with initial shales. Oil P* is the potential contribution of the increased pore volume to storing the extracted oil, which is calculated by $Oil\ P^* = 100\% \cdot (V_{Ext\ p} - V_{Ini\ p})/V_{oil}$, where $V_{Ext\ p}$ is the pore volume of shale after extraction, $V_{Ini\ p}$ is the pore volume of initial shale, and V_{oil} is the extracted oil volume (Table 1). Oil P* was only calculated for BS3 and GH4 since these are the only shales containing oil generated by maturation.

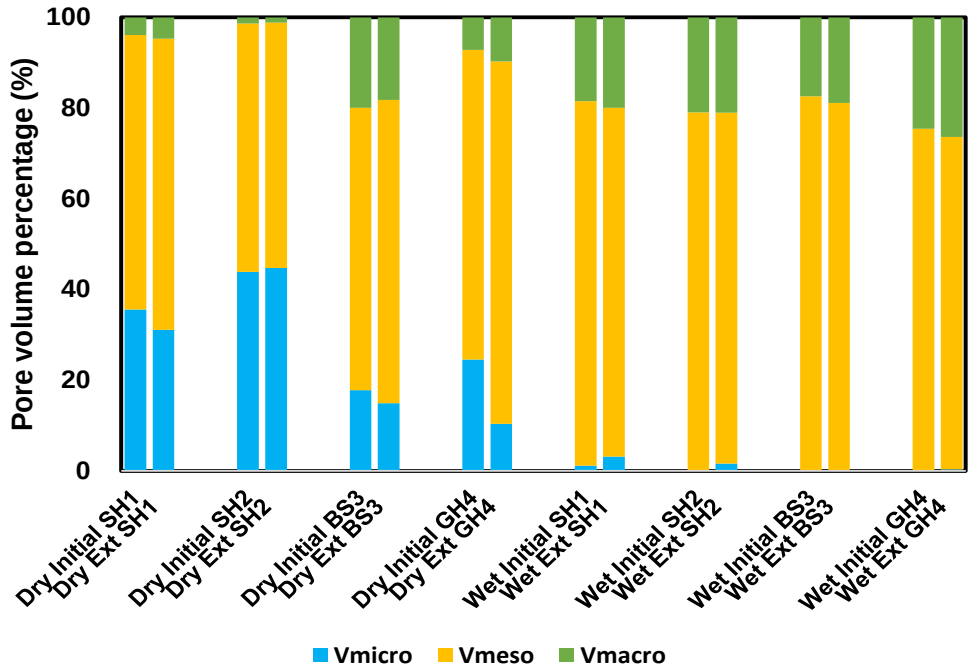

Figure 2. Micropore, mesopore, and macropore (<100 nm) volume percentages for the dry and wet initial and extracted shales.

The influence of solvent extraction is much larger for the two lower maturity shales. Table 2 indicates that the SA doubled from 0.13 to 0.26 m^2/g for dry BS3 and increased by 20% from 2.19 to 2.62 m^2/g for GH4. The total nanopore volume (up to 100 nm) also doubled for dry BS3 (from 0.55 to 1.1 µL/g) and increased by 176% for GH4 (from 2.4 to 6.7 µL/g). If the increased 64% micropore pore volume is generated solely by removing the oil, it is estimated that 9% of the extracted oil in shale BS3 is stored in the micropores (Oil p* in Table 2). The mesopores (from 0.34 to 0.72 µL/g) and macropores up to 100 nm (from 0.11 to 0.20 µL/g) increase by 110 and 78%, respectively, after oil extraction. This new porosity provides estimated storage space for 52 and 12%, respectively, of the extracted oil (64% in total). Similarly, for GH4, the increase of 17% micropore volume provides storage space for 23% oil, with the rest 77% oil stored in the mesopore or/and macropore, since the mesopores (from 1.7 to 5.3 µL/g) and 50-100 nm macropores volume (from 0.17 to 0.7 µL/g) increase by over 200% (Table 2). Clearly, for GH4, oil removal opens access to blocked meso/macropores since the increase in pore volume is considerably greater than the volume of the extracted oil. For BS3, where the increase in pore volume accounts for 73% of the extracted oil, the implication is that some of the oil resides in pores >100 nm.

The aliphatic and aromatic hydrocarbons in oils are mainly stored in micro and mesopores, but the higher molecular mass polar species and asphaltenes reside primarily in the macropores [11, 23, 28, 68]. The increase in macropore volume for the extracted shale is consistent with the non-hydrocarbons being removed by solvent extraction. The overall nanoporosity increases after extraction for the oil-window shale, BS3, and the gas-window shale, GH4 are larger than SH1 and SH2 since it is oil generated by maturation being extracted, as opposed to drilling fluids residing close to the surface.

As expected from our earlier studies [5, 8], most pore volume and SA are lost on wetting the shales (Table 2). Although mesopores are still dominant as for the dry shales, macropores replace micropores as the secondary pores in the wet shales (Figure 2), for both the initial and extracted samples. This arises from most of the micropores or micropore-necks being filled or/and blocked by water [5]. Solvent extraction provides a more complex influence on the pore system of wet shales. For extracted wet over-mature shales, SH1 and SH2, apart from micropore volume increasing (from 0.0039 to 0.0081 μL/g for wet SH1, and from 0 to 0.0033 μL/g for wet SH2), the mesopore, macropore and nanopore pore volumes all decrease slightly, with the reduction of -28, -19 and -25% for SH1, and -26, -25, -25% for SH2 (Table 2). The increase of micropores indicates there is less water to fill or block micropores in the extracted shales than initial shales as oil extraction did not enlarge micropores, mesopore, or macropores as discussed above. Larger micropores in extracted wet SH1 and SH2 could be due to the solvent interacting and altering the pore surface [11, 12, 28, 69], making it hard for water to condense or block micropores in solvent-extracted shales than initial shales. Additionally, the moisture contents of the extracted shales are also less than those of the initial shales (Table 1), with reductions of 15, 7, 37, and 25% for wet SH1, SH2, BS3, and GH4, respectively, suggesting less water is absorbed.

For the wet BS3 and GH4 shales, apart from the micropore volume of BS3 remaining close to zero, all the other pore volumes display increases after solvent extraction (Table 2). These increases are 80% for mesopores (from 0.18 to 0.32 μL/g), 98% for macropores (from 0.038 to 0.07 μL/g) and 83% for the total nanopores (from 0.22 to 0.40 μL/g) volumes for wet BS3. Large proportional increases are observed for GH4, the micropores increase from 0 to 0.0012 μL/g, being 257% for mesopores (from 0.07 to 0.25 μL/g), 295% for macropores (from 0.023 to 0.089 μL/g) and 268% total nanopores (from 0.09 to 0.34 μL/g). The increases in wet shales show a similar pattern to the dry samples. The

329 pore volume increases for the wet extracted BS3 and GH4 shales are due to a combination of oil
330 removal enlarging the pores and the extracted shales having lower moisture contents.

331 Overall, the results indicate that extracted oil as well as water can have significant impact on pore
332 characteristics. Although overmature shales have the largest pore volume, almost no oil remains, as
333 most of the oil has migrated. The limited pore system changes of overmature shales upon solvent
334 extraction indicates the original pore system is not changing to any significant degree, with only the
335 interactions on the shale pore surface being modified. The oil generated by maturation mainly
336 resides in the pores <50 nm (micropores and mesopores) for the early to high mature shales, and
337 removing the oil increases the accessible pore volume for both the dry or wet shales.

338 ### 3.4 Impact of solvent extraction on methane adsorption

339 The methane adsorption isotherms of the initial and solvent extracted shales are compared in
340 Figures 3 and 4, for the dry and moisture-equilibrated samples, respectively. The equilibrium
341 methane adsorption capacities (Qm) derived from the isotherms are listed in Table 3. For the initial
342 samples, the solubility of methane in oils has been estimated by Henry's Law, assuming that the
343 methane is accessible to all the extractable oil. Thus, the estimated amount of adsorbed methane
344 after Henry's law is the difference between the total amount of methane taken up by the samples
345 and the dissolved methane estimated by Henry's Law linear plots in Figures 3 and 4. For the dry
346 samples, the two over-mature shales, SH1 and SH2, have the higher equilibrium adsorption
347 capacities, 77 and 127 mg/g TOC, respectively, compared to 16 and 21 mg/g TOC, respectively for
348 the oil and gas window shales, BS3 and GH4, for the dry samples (Figure 3).

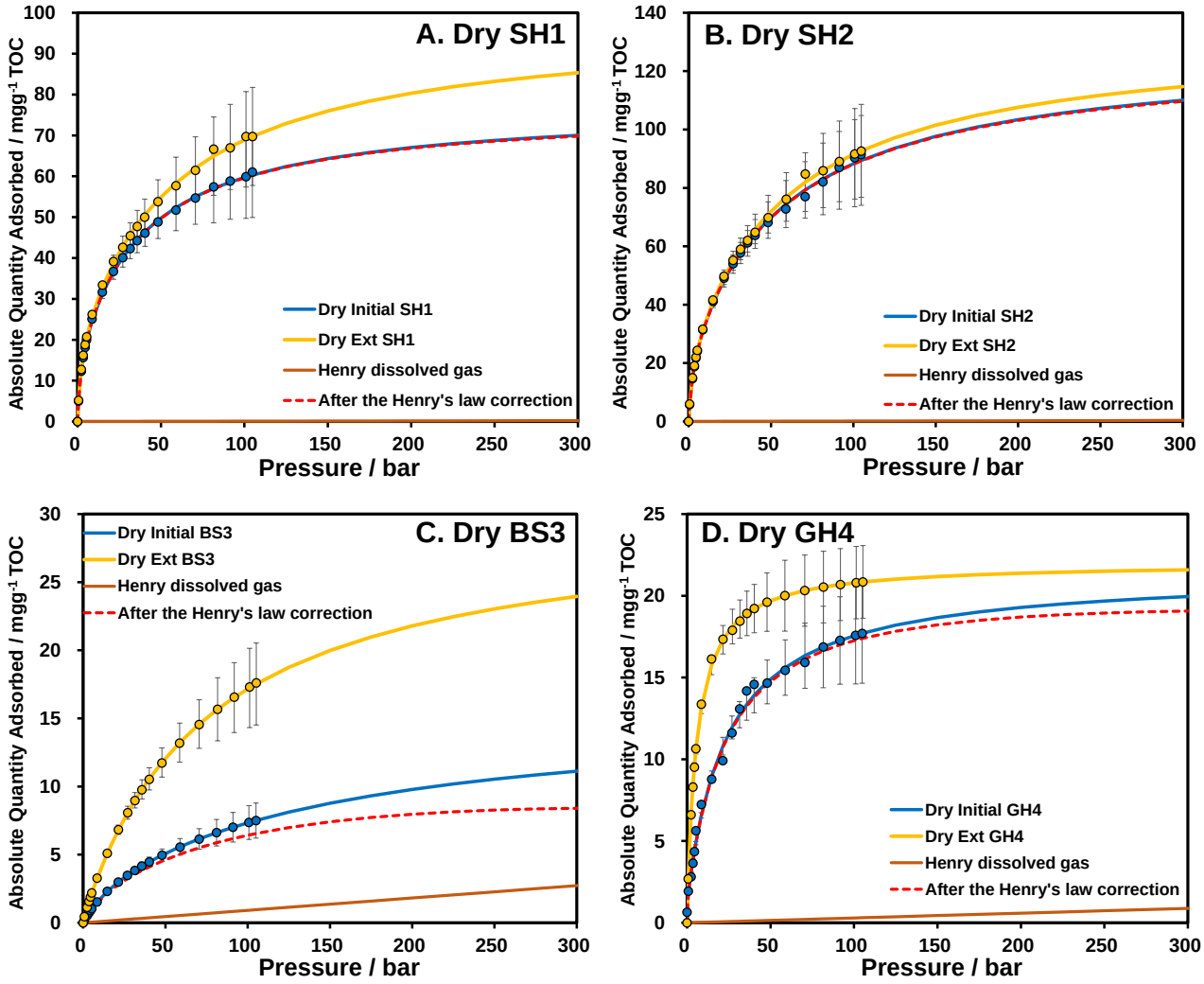

Figure 3. Methane adsorption isotherms of the dry initial and extracted shales, after the Henry's law correction for initial shales, and the dissolved methane uptakes calculated by Henry's Law.

Shales SH1, SH2, and BS3 have type I(b) isotherms, with shale GH4 having a type I(a) isotherm displaying a steeper isotherm at low pressures (Figure 3), arising mainly from narrow micropores (width <1 nm) [43]. For overmature dry shales, SH1 and SH2 (Figures 3A and B), although the average methane adsorption isotherms of extracted shales are higher than the initial shales, with the Qm increasing by 27% (from 77 to 98 mg/g TOC) for SH1 and 5% (from 127 to 133 mg/g TOC) for SH2. They are still within the error range, suggesting the methane adsorption capacities of initial and extracted shales are relatively close. Thus, solvent extraction shows little impact on their methane adsorption capacities. Further, even deducting the potential contribution from dissolved methane in the low yields of extracted oil, the methane adsorption isotherms after the Henry's Law correction

has very little impact. With the methane adsorption amount at 300 bar (Q_{300bar} was used as there is no Qm for henry law) changing by only *ca*. 0.3% for SH1 (from 70.0 to 69.8 mg/g TOC) and SH2 (from 110.0 to 109.6 mg/g TOC).

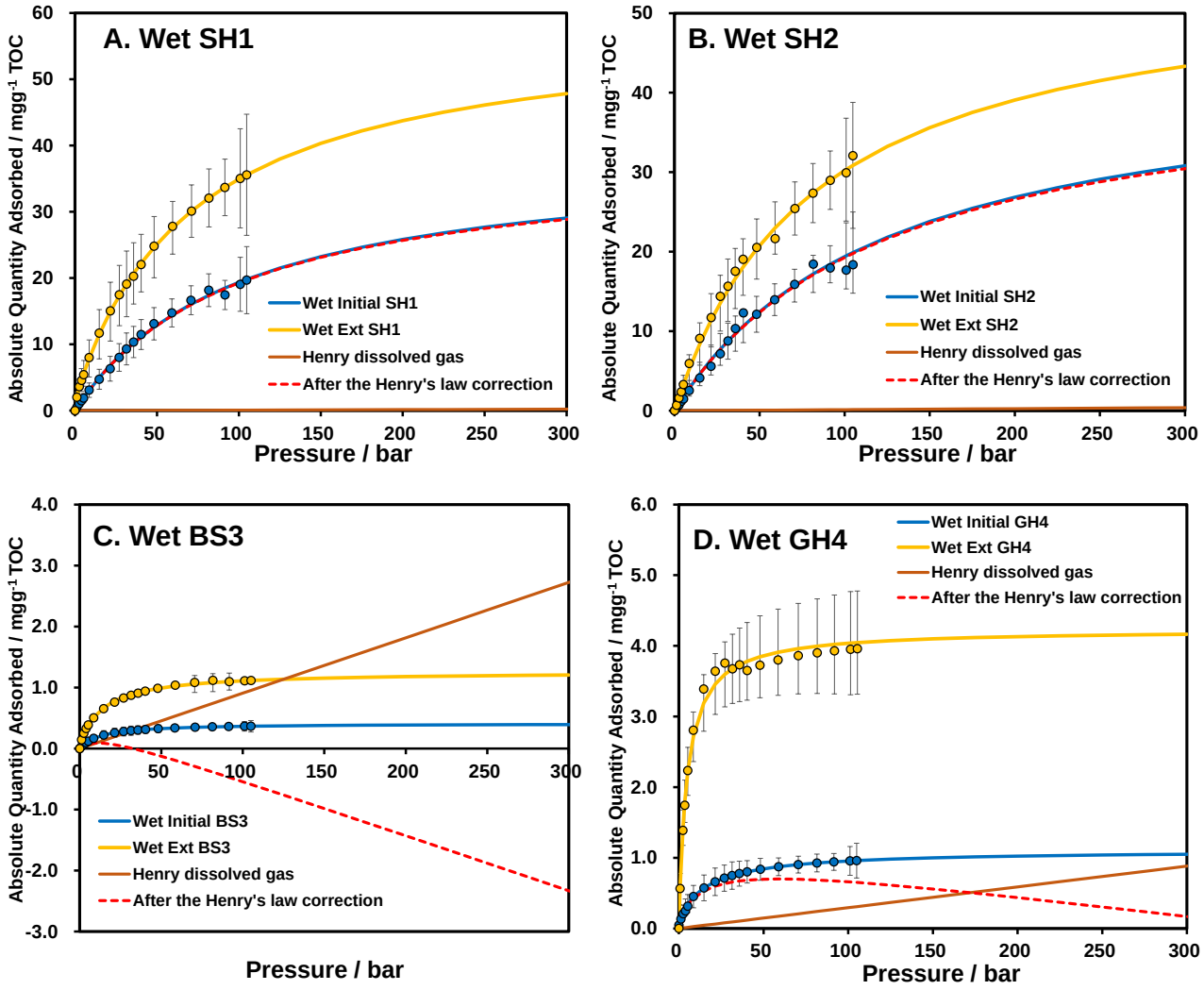

Figure 4. Methane adsorption isotherms of the wet initial and extracted shales, showing the Henry's Law corrections for dissolved methane in the oil present.

In contrast to the overmature shales, removing the residual oil increases the methane adsorption capacities of dry oil-window shale BS3 significantly (Qm increased by 90% from 16 to 30 mg/g TOC). A smaller increase was observed for dry gas-window shale GH4 (Qm increased by 3% from 21 to 22 mg/g TOC) consistent with the lower yield of extractable oil compared to BS3. A steeper uptake at low pressure (<50 bar) of extracted GH4 isotherm was observed (Figure 3D), which indicates removing extracted GH4 oil increases narrow micropores (<1 nm) [43], consistent with the oil being

relatively light (section 3.2). Although isotherms are less steep after the Henry's Law correction for dry shales, the isotherm type remains the same, with their shapes being similar in the low-pressure range (<50 bar, Figure 3). The Henry's Law corrections reduce Q_{300bar} for BS3 (from 11.1 to 8.4 mg/g TOC) (Figure 3C) and GH4 (from 20.0 to 19.1 mg/g TOC) (Figure 3D) by 25 and 4.4%, respectively. However, this assumes that all the oil is accessible to the methane, if this is not the case, the impact of dissolved methane will be much less.

Table 3. The methane adsorption amount of dry, wet, initial, and extracted shales.

Adsorption (mg/g TOC)	Initial SH1	Ext SH1	*Qm change SH1 (%)*	Initial SH2	Ext SH2	*Qm change SH2 (%)*	Initial BS3	Ext BS3	*Qm change BS3 (%)*	Initial GH4	Ext GH4	*Qm change GH4 (%)*
Dry Q_{300bar}	70.0	85.3	-	110.0	114.7	-	11.1	24.0	-	20.0	21.6	-
Dry Qm	77	98	***27***	127	133	***5***	16	30	***90***	21	22	***3***
Wet Q_{300bar}	29.1	47.8	**-**	30.8	43.3	**-**	0.4	1.2	**-**	1.1	4.2	**-**
Wet Qm	39	59	***52***	44	55	***27***	0.4	1.3	***207***	1.1	4.2	***282***
Qm Reduction (%)	**50**	**40**	**-**	**66**	**58**	**-**	**97**	**96**	**-**	**95**	**81**	**-**

Qm is the equilibrium methane adsorption capacities; Q_{300bar} is the methane adsorption amount at 300 bar; Q change (%) is the methane adsorption amount changes before and after the extraction; Qm Reduction (%) is the methane adsorption reduction for wet samples compared with corresponding dry shales.

Methane adsorption capacities of both the initial and extracted shales are reduced after moisture equilibration due to micropores being blocked (Table 3) [5]. The reductions in Qm for the initial shales, SH1, SH2, BS3, and GH4 are 50, 66, 97, and 95%, respectively, which are larger than the extracted samples (40, 58, 96, and 81%, respectively), suggesting moisture has a slightly reduced impact for the extracted shales since they adsorbed less water (Table 1). Additionally, the methane adsorption capacities for the wet extracted shales are larger than for the initial shales (Table 3), even considering the experimental errors (Figure 4). The Qm of wet extracted SH1 increased (from 39 to 59 mg/g TOC), SH2 (from 44 to 55mg/g TOC), BS3 (from 0.4 to 1.3 mg/g TOC), and GH4 (from 1.1 to 4.2 mg/g TOC), representing increases of 52, 27, 207 and 282% compared to the wet initial shales (Table 3). These are consistent with the increase of accessible micropore volume for the extracted shales (Section 3.3).

For wet overmature shales, SH1 and SH2, the Henry's Law corrections for dissolved gas had virtually no effect on the methane sorption capacities (Figure 4A and 4B). In contrast, the methane adsorption isotherms after the Henry's Law corrections decrease with increasing pressure and go negative for BS3 and GH4 at the pressure of ca. 40 and 300 bar, respectively (Figure 4C, and 4D). This indicates that virtually none of the methane is accessible to the oil. This arises from water blocking the micropores or micropore necks. For both BS3 and GH4, solvent extraction significantly increases the methane adsorption capacities, by a factor of 3-4, compared to the initial moisture equilibrated shales by reducing the extent to which the pores are blocked by water.

4. GIP estimation

Understanding both the impact of extracted oil and moisture on porosity and gas adsorption properties is vital for an accurate evaluation of shale gas resources and the design of effective production strategies. Like moisture, the removal of oil generated by maturation can lead to an overestimation of GIP [5]. The GIP can be estimated from the shale gas holding capacity which is calculated based on the free gas from porosity and adsorbed gas from high-pressure methane adsorption [1, 5, 8]. Equation (4) has been used to calculate GIP in this study. The porosities of the dry and wet shale used for calculating the free gas are based on Equations (5) and (6). Considering the buried depths of the four samples, the reservoir pressure and temperature for the overmature shales, SH1 and SH2, are estimated as 600 bar and 100 °C, for the UK Bowland shales, BS3, 300 bar and 60 °C and GH4, 450 bar and 80 °C [1, 5, 70]. The excess adsorbed gas content reduced by 45, 35, and 25 % at 100, 80, and 60 °C when compared with 25 °C [7, 71, 72].

$$GIP = Q_{free} + Q_a = Q_{free} + Q_e + V_a \times \rho_g = V_{tot} \times \rho_g + Q_e \quad (4)$$

$$Porosity_{dry} = \frac{V_{dry\ pore}}{V_{sh}} = 1 - \frac{\rho_{dry\ bulk}}{\rho_{dry\ sk}} \quad (5)$$

$$Porosity_{wet} = \frac{V_{wet\ pore}}{V_{sh}} = 1 - \frac{\rho_{wet\ bulk}}{\rho_{wet\ sk}} = 1 - \frac{\rho_{dry\ bulk}}{\rho_{wet\ sk}} \times (1 + W) \quad (6)$$

Where, Q_{free} is the free gas; Q_a is the absolute adsorption gas; Q_e is the excess adsorption gas; V_a is the pore volume for gas to adsorb into; ρ_g is the density of the bulk gas, which can be obtained from the REFPROP version 8.0 software; V_{tot} is the total pore volume accessible to gas in shale; $Porosity_{dry}$ is the total porosity of dry shale; $V_{dry\ pore}$ is the pore volume of dry shale; $Porosity_{wet}$ is the total porosity of wet shale; $V_{wet\ pore}$ is the pore volume of wet shale; V_{sh} is the shale sample volume; $\rho_{wet\ bulk}$ is the bulk density of wet shale, $\rho_{dry\ bulk}$ is the bulk density of dry shales from mercury intrusion porosimetry (MIP) at 0.035 bar, $\rho_{dry\ sk}$ and $\rho_{wet\ sk}$ are the skeletal densities of the dry and wet samples obtained from helium pycnometry; W is the moisture content.

The total porosity and GIPs estimated for the initial and extracted shales are compared in Table 4. Oil extraction increased the total porosity from 18.3 to 21.0% for the dry shales, BS3, and increases from 16.8 to 20.9% for the moisture equilibrated shale, which are much larger increases than the other shales, as BS3 has the highest oil yield (Table 4). Table 4 indicates that the estimated GIP increases with total porosity, in the order of GH4>BS3>SH1>SH2 for the initial shales under both dry and moisture equilibrated conditions. Although SH1 and SH2 have much larger adsorbed gas (Q_a) contributions, the free gas (Q_{free}) contributions controlled by the total pore volume are smaller than for BS3 and GH4 (Table 3). However, in all cases, the free gas contributions dominate the GIP estimates for the initial dry shales (82, 65, 99, and 98% for SH1, SH2, BS3, and GH4, respectively, Table 4). As expected, the GIP estimated for the moisture equilibrated shales are lower than for dry shales, with reductions of 32, 38, 11, and 12% observed for initial SH1, SH2, BS3, and GH4, respectively, with the reductions for the extracted moisture equilibrated shales being 27, 28, 4 and 14%, respectively, when compared with the corresponding extracted dry shales (Table 4). This confirms that the GIP based on dry shales is significantly overestimated, as previous research indicated [5, 73, 74]. Moreover, moisture reduces the adsorbed gas (41-96%) more than the free gas (2-27%) for both the initial and extracted shale (Table 4) since the impact of moisture is mainly blocking micropores for adsorbed gas rather than the larger pores accommodating most of the free gas.

444 Table 4. The porosity, total pore volume, and the estimated GIP of the initial and extracted shales.

Sample name	Porosity (%)	V_{total} (m^3/t)	Q_a (kg/t)	Q_{free} (kg/t)	GIP (kg/t)	GIP change after extraction (%)
Dry Initial SH1	10.2	0.0432	2.1	9.3	11.4	6
Dry Ext SH1	10.2	0.0434	2.6	9.5	12.1	
Dry Initial SH2	4.0	0.0156	1.6	2.9	4.5	-3
Dry Ext SH2	3.8	0.0148	1.7	2.7	4.4	
Dry Initial BS3	18.3	0.0857	0.21	15.5	15.7	16
Dry Ext BS3	21.0	0.1008	0.44	18.2	18.7	
Dry Initial GH4	22.2	0.1046	0.44	22.8	23.2	3
Dry Ext GH4	22.8	0.1080	0.47	23.5	23.9	
Wet Initial SH1	6.8	0.0284	0.94	6.8	7.8	12
Wet Ext SH1	7.2	0.0304	1.5	7.3	8.8	
Wet Initial SH2	2.5	0.0095	0.49	2.3	2.8	11
Wet Ext SH2	2.7	0.0102	0.65	2.5	3.1	
Wet Initial BS3	16.8	0.0772	0.007	14.0	14.0	22
Wet Ext BS3	20.9	0.0990	0.022	17.9	18.0	
Wet Initial GH4	20.3	0.0930	0.023	20.3	20.3	1
Wet Ext GH4	20.2	0.0938	0.090	20.5	20.6	

445 V_{total} is the total pore volume calculated from the porosity of corresponding shales.

446 Overall, the changes arising from oil extraction are relatively small for the two overmature shales,
447 SH1, SH2, and the gas window shale, GH4 (-3 to 6% for the dry shales and 1-12% for the moisture
448 equilibrated shales, Table 4) with the largest changes being for the oil window shale, BS3. In contrast,
449 Table 4 indicates that the GIP is overestimated by 16 and 22% for both dry and moisture equilibrated
450 extracted oil window shale, BS3.

451 Clearly, the impact of solvent extraction on the estimated GIP is minimal for the two overmature
452 shales investigated, especially compared to moisture (Table 4). In contrast, although some
453 researchers believe removing oil in low maturity shale has little influence on methane adsorption
454 [23], the impact of oil removal is significant for oil-window shales, with the GIP being over-estimated
455 by 22% for the shale investigated in this study. For such shales, a combination of moisture
456 equilibration and not extracting oil present generated by maturation is essential to obtain reliable
457 GIP estimates.

5. Conclusions

1). Solvent extraction has limited impact on the methane adsorption and pore texture for the dry overmature shales, SH1 and SH2, with the small amounts of extractable oil arising from drilling mud contamination. However, micropore volume and the methane adsorption capacities for the wet over mature shales increased after solvent extraction, possibly due to the reductions in moisture content, meaning that there is reduced pore blocking.

2). More than 60% of the extractable oil resides in micro and mesopores for the oil-window BS3. Removing the oil increased the nano, micro, meso, and macropore volumes by nearly 300% for the dry BS3 and GH4. The increases in methane adsorption capacities are proportionally greater for the wet shales (207-282%) compared to the dry shales (90 and 3%).

3). Henry's Law estimations have indicated that the proportions of dissolved gas in the dry shale samples is very small. For wet shales, not all the residual oil is accessible if water blocks some of the micropores, which means the dissolved gas calculated by Henry's Law could be significantly overestimated.

4). Solvent extraction increases the estimated GIP by 16% for the dry oil-window shale, BS3, and moisture reduces the GIP of the initial BS3 shale by 11%. The GIP for extracted wet shale is overestimated by 22%. The impact on GIP estimates was considerably less for the over-mature shales due to their low extractable oil contents. Nevertheless, this study indicates the significant impact that natural oil arising from maturation can have on the estimated GIP for oil-window shales.

Acknowledgments

The authors greatly acknowledge financial support from the National Environment Research Council (Grant no: NE/C507002/1) and the Faculty of Engineering Research Excellence Ph.D. Scholarship for

Wei Li provided by the University of Nottingham. The British Geological Survey is acknowledged for providing the cores for the UK shales.

References

[1] Tang X, Ripepi N, Stadie NP, Yu L, Hall MR. A dual-site Langmuir equation for accurate estimation of high pressure deep shale gas resources. Fuel 2016;185:10-7.
[2] Curtis JB. Fractured shale-gas systems. AAPG bulletin 2002;86(11):1921-38.
[3] Ross DJ, Bustin RM. Shale gas potential of the lower Jurassic Gordondale member, northeastern British Columbia, Canada. Bulletin of Canadian Petroleum Geology 2007;55(1):51-75.
[4] Ross DJ, Bustin RM. The importance of shale composition and pore structure upon gas storage potential of shale gas reservoirs. Marine and petroleum Geology 2009;26(6):916-27.
[5] Li W, Stevens LA, Uguna CN, Vane CH, Meredith W, Tang L, et al. Comparison of the impact of moisture on methane adsorption and nanoporosity for over mature shales and their kerogens. International Journal of Coal Geology 2021:103705.
[6] Gasparik M, Bertier P, Gensterblum Y, Ghanizadeh A, Krooss BM, Littke R. Geological controls on the methane storage capacity in organic-rich shales. International Journal of Coal Geology 2014;123:34-51.
[7] Rexer TF, Benham MJ, Aplin AC, Thomas KM. Methane adsorption on shale under simulated geological temperature and pressure conditions. Energy & Fuels 2013;27(6):3099-109.
[8] Whitelaw P, Uguna CN, Stevens LA, Meredith W, Snape CE, Vane CH, et al. Shale gas reserve evaluation by laboratory pyrolysis and gas holding capacity consistent with field data. Nature communications 2019;10(1):1-10.
[9] DiStefano VH, McFarlane J, Stack AG, Perfect E, Mildner DF, Bleuel M, et al. Solvent-pore interactions in the Eagle Ford shale formation. Fuel 2019;238:298-311.
[10] Mohnhoff D, Littke R, Krooss BM, Weniger P. Flow-through extraction of oil and gas shales under controlled stress using organic solvents: Implications for organic matter-related porosity and permeability changes with thermal maturity. International Journal of Coal Geology 2016;157:84-99.
[11] Qi Y, Ju Y, Cai J, Gao Y, Zhu H, Hunag C, et al. The effects of solvent extraction on nanoporosity of marine-continental coal and mudstone. Fuel 2019;235:72-84.
[12] Cao Y, Han H, Liu H-w, Jia J-c, Zhang W, Liu P-w, et al. Influence of solvents on pore structure and methane adsorption capacity of lacustrine shales: An example from a Chang 7 shale sample in the Ordos Basin, China. Journal of Petroleum Science and Engineering 2019;178:419-28.
[13] Barker F. Trondhjemite: definition, environment and hypotheses of origin. Developments in petrology. Elsevier; 1979, p. 1-12.
[14] Eldridge RB. Oil contaminant removal from drill cuttings by supercritical extraction. Industrial & engineering chemistry research 1996;35(6):1901-5.
[15] Bernard S, Horsfield B. Thermal maturation of gas shale systems. Annual Review of Earth and Planetary Sciences 2014;42:635-51.
[16] Dayal AM, Mani D. Shale gas: Exploration and environmental and economic impacts. Elsevier; 2017.
[17] Tissot BP, Welte DH. Petroleum formation and occurrence. Springer Science & Business Media; 2013.
[18] Rexer TF, Mathia EJ, Aplin AC, Thomas KM. High-pressure methane adsorption and characterization of pores in Posidonia shales and isolated kerogens. Energy & Fuels 2014;28(5):2886-901.
[19] Guo S. Experimental study on isothermal adsorption of methane gas on three shale samples from Upper Paleozoic strata of the Ordos Basin. Journal of Petroleum Science and Engineering 2013;110:132-8.

[20] Wang Y, Zhu Y, Liu S, Zhang R. Pore characterization and its impact on methane adsorption capacity for organic-rich marine shales. Fuel 2016;181:227-37.
[21] Löhr S, Baruch E, Hall P, Kennedy M. Is organic pore development in gas shales influenced by the primary porosity and structure of thermally immature organic matter? Organic Geochemistry 2015;87:119-32.
[22] Hu H, Zhang T, Wiggins-Camacho JD, Ellis GS, Lewan MD, Zhang X. Experimental investigation of changes in methane adsorption of bitumen-free Woodford Shale with thermal maturation induced by hydrous pyrolysis. Marine and Petroleum Geology 2015;59:114-28.
[23] Liu G, Huang Z, Jiang Z, Chen J, Chen F, Xing J. Gas adsorption capacity calculation limitation due to methane adsorption in low thermal maturity shale: A case study from the Yanchang Formation, Ordos Basin. Journal of Natural Gas Science and Engineering 2016;30:106-18.
[24] Ibad SM, Padmanabhan E. Methane sorption capacities and geochemical characterization of Paleozoic shale Formations from Western Peninsula Malaysia: Implication of shale gas potential. International Journal of Coal Geology 2020:103480.
[25] Guo H, Jia W, Lei Y, Luo X, Cheng M, Wang X, et al. The composition and its impact on the methane sorption of lacustrine shales from the Upper Triassic Yanchang Formation, Ordos Basin, China. Marine and Petroleum Geology 2014;57:509-20.
[26] Berthezene N, De Hemptinne J-C, Audibert A, Argillier J-F. Methane solubility in synthetic oil-based drilling muds. Journal of Petroleum Science and Engineering 1999;23(2):71-81.
[27] Jarrett AJ, Schinteie R, Hope JM, Brocks JJ. Micro-ablation, a new technique to remove drilling fluids and other contaminants from fragmented and fissile rock material. Organic geochemistry 2013;61:57-65.
[28] DiStefano VH, McFarlane J, Anovitz LM, Stack AG, Gordon AD, Littrell KC, et al. Extraction of organic compounds from representative shales and the effect on porosity. Journal of Natural Gas Science and Engineering 2016;35:646-60.
[29] Li W, Pang X, Snape C, Zhang B, Zheng D, Zhang X. Molecular Simulation Study on Methane Adsorption Capacity and Mechanism in Clay Minerals: Effect of Clay Type, Pressure, and Water Saturation in Shales. Energy & Fuels 2019;33(2):765-78.
[30] Tan J, Weniger P, Krooss B, Merkel A, Horsfield B, Zhang J, et al. Shale gas potential of the major marine shale formations in the Upper Yangtze Platform, South China, Part II: Methane sorption capacity. Fuel 2014;129:204-18.
[31] Simpson J, Dearing H. Diffusion Osmosis-An unrecognized cause of shale instability. *IADC/SPE Drilling Conference.* Society of Petroleum Engineers; 2000.
[32] Loucks RG, Ruppel SC. Mississippian Barnett Shale: Lithofacies and depositional setting of a deep-water shale-gas succession in the Fort Worth Basin, Texas. AAPG bull 2007;91(4):579-601.
[33] Heller R, Zoback M. Adsorption of methane and carbon dioxide on gas shale and pure mineral samples. Journal of Unconventional Oil and Gas Resources 2014;8:14-24.
[34] Jin Z, Firoozabadi A. Effect of water on methane and carbon dioxide sorption in clay minerals by Monte Carlo simulations. Fluid Phase Equilibria 2014;382:10-20.
[35] Ji L, Zhang T, Milliken KL, Qu J, Zhang X. Experimental investigation of main controls to methane adsorption in clay-rich rocks. Applied Geochemistry 2012;27(12):2533-45.
[36] Zolfaghari A, Dehghanpour H, Xu M. Water sorption behaviour of gas shales: II. Pore size distribution. International Journal of Coal Geology 2017;179:187-95.
[37] Merkel A, Fink R, Littke R. High pressure methane sorption characteristics of lacustrine shales from the Midland Valley Basin, Scotland. Fuel 2016;182:361-72.
[38] Young JF. Humidity control in the laboratory using salt solutions—a review. Journal of Applied Chemistry 1967;17(9):241-5.
[39] Zolfaghari A, Dehghanpour H, Holyk J. Water sorption behaviour of gas shales: I. Role of clays. International Journal of Coal Geology 2017;179:130-8.
[40] Greenspan L. Humidity fixed points of binary saturated aqueous solutions. Journal of research of the national bureau of standards 1977;81(1):89-96.
[41] Schoenherr J, Littke R, Urai JL, Kukla PA, Rawahi Z. Polyphase thermal evolution in the Infra-Cambrian Ara Group (South Oman Salt Basin) as deduced by maturity of solid reservoir bitumen. Organic Geochemistry 2007;38(8):1293-318.

[42] Brunauer S, Emmett PH, Teller E. Adsorption of gases in multimolecular layers. Journal of the American chemical society 1938;60(2):309-19.
[43] Thommes M, Kaneko K, Neimark AV, Olivier JP, Rodriguez-Reinoso F, Rouquerol J, et al. Physisorption of gases, with special reference to the evaluation of surface area and pore size distribution (IUPAC Technical Report). Pure and Applied Chemistry 2015;87(9-10):1051-69.
[44] Rouquerol J, Llewellyn P, Rouquerol F. Is the BET equation applicable to microporous adsorbents. Stud Surf Sci Catal 2007;160(07):49-56.
[45] Qi L, Tang X, Wang Z, Peng X. Pore characterization of different types of coal from coal and gas outburst disaster sites using low temperature nitrogen adsorption approach. International Journal of Mining Science and Technology 2017;27(2):371-7.
[46] Bertier P, Schweinar K, Stanjek H, Ghanizadeh A, Clarkson CR, Busch A, et al. On the use and abuse of N2 physisorption for the characterization of the pore structure of shales. *The clay minerals society workshop lectures series.* 21. 2016:151-61.
[47] Luo P, Zhong N, Khan I, Wang X, Wang H, Luo Q, et al. Effects of pore structure and wettability on methane adsorption capacity of mud rock: Insights from mixture of organic matter and clay minerals. Fuel 2019;251:551-61.
[48] Gregg S, Sing K. W. Adsorption, surface area and porosity. London: Academic Press 1982:195-7.
[49] Liu J, Sun N, Sun C, Liu H, Snape C, Li K, et al. Spherical potassium intercalated activated carbon beads for pulverised fuel CO2 post-combustion capture. Carbon 2015;94:243-55.
[50] Okolo GN, Everson RC, Neomagus HW, Roberts MJ, Sakurovs R. Comparing the porosity and surface areas of coal as measured by gas adsorption, mercury intrusion and SAXS techniques. Fuel 2015;141:293-304.
[51] Sircar S. Gibbsian surface excess for gas adsorption revisited. Industrial & engineering chemistry research 1999;38(10):3670-82.
[52] Stasiuk L, Snowdon L. Fluorescence micro-spectrometry of synthetic and natural hydrocarbon fluid inclusions: crude oil chemistry, density and application to petroleum migration. Applied Geochemistry 1997;12(3):229-41.
[53] Hanafy H, Macary S, ElNady Y, Bayomi A, El Batanony M. A new approach for predicting the crude oil properties. *SPE Production Operations Symposium.* Society of Petroleum Engineers; 1997.
[54] Zou C, Dong D, Wang S, Li J, Li X, Wang Y, et al. Geological characteristics and resource potential of shale gas in China. Petroleum exploration and development 2010;37(6):641-53.
[55] Andrews IJ. The Carboniferous Bowland Shale gas study: geology and resource estimation. 2013.
[56] Clarke H, Turner P, Bustin RM, Riley N, Besly B. Shale gas resources of the Bowland Basin, NW England: a holistic study. Petroleum Geoscience 2018;24(3):287-322.
[57] Wenger LM, Davis CL, Evensen JM, Gormly JR, Mankiewicz PJ. Impact of modern deepwater drilling and testing fluids on geochemical evaluations. Organic geochemistry 2004;35(11-12):1527-36.
[58] Curtis ME, Cardott BJ, Sondergeld CH, Rai CS. Development of organic porosity in the Woodford Shale with increasing thermal maturity. International Journal of Coal Geology 2012;103:26-31.
[59] Gasparik M, Ghanizadeh A, Bertier P, Gensterblum Y, Bouw S, Krooss BM. High-pressure methane sorption isotherms of black shales from the Netherlands. Energy & fuels 2012;26(8):4995-5004.
[60] Hu H. Methane adsorption comparison of different thermal maturity kerogens in shale gas system. Chinese Journal of Geochemistry 2014;33(4):425-30.
[61] Mastalerz M, Hampton L, Drobniak A, Loope H. Significance of analytical particle size in low-pressure N2 and CO2 adsorption of coal and shale. International Journal of Coal Geology 2017;178:122-31.
[62] Cao T, Song Z, Wang S, Xia J. A comparative study of the specific surface area and pore structure of different shales and their kerogens. Science China Earth Sciences 2015;58(4):510-22.

[63] Tissot B. Recent advances in petroleum geochemistry applied to hydrocarbon exploration. AAPG Bulletin 1984;68(5):545-63.
[64] Katsube T. Shale permeability and pore-structure evolution characteristics. Natural Resources Canada, Geological Survey of Canada; 2000.
[65] Best M, Katsube T. Shale permeability and its significance in hydrocarbon exploration. The Leading Edge 1995;14(3):165-70.
[66] Alfi M, Barrufet M, Killough J. Effect of pore sizes on composition distribution and enhance recovery from liquid shale—Molecular sieving in low permeability reservoirs. Fuel 2019;235:1555-64.
[67] Lee S, Fischer TB, Stokes MR, Klingler RJ, Ilavsky J, McCarty DK, et al. Dehydration effect on the pore size, porosity, and fractal parameters of shale rocks: Ultrasmall-angle X-ray scattering study. Energy & fuels 2014;28(11):6772-9.
[68] Chen J, Xiao X. Evolution of nanoporosity in organic-rich shales during thermal maturation. Fuel 2014;129:173-81.
[69] Job N, Théry A, Pirard R, Marien J, Kocon L, Rouzaud J-N, et al. Carbon aerogels, cryogels and xerogels: Influence of the drying method on the textural properties of porous carbon materials. Carbon 2005;43(12):2481-94.
[70] Li J, Zhou S, Gaus G, Li Y, Ma Y, Chen K, et al. Characterization of methane adsorption on shale and isolated kerogen from the Sichuan Basin under pressure up to 60 MPa: Experimental results and geological implications. International Journal of Coal Geology 2018;189:83-93.
[71] Zou J, Rezaee R, Liu K. Effect of temperature on methane adsorption in shale gas reservoirs. Energy & Fuels 2017;31(11):12081-92.
[72] Ji W, Song Y, Jiang Z, Chen L, Li Z, Yang X, et al. Estimation of marine shale methane adsorption capacity based on experimental investigations of Lower Silurian Longmaxi formation in the Upper Yangtze Platform, south China. Marine and Petroleum Geology 2015;68:94-106.
[73] Chalmers GR, Bustin MR. PS The Effects and Distribution of Moisture in Gas Shale Reservoir Systems. AAPG Annual Convention and Exhibition 2010.
[74] Krooss Bv, Van Bergen F, Gensterblum Y, Siemons N, Pagnier H, David P. High-pressure methane and carbon dioxide adsorption on dry and moisture-equilibrated Pennsylvanian coals. International Journal of Coal Geology 2002;51(2):69-92.